

**SUPRAMOLECULAR ASSEMBLIES
IN AN UNPRECEDENTED ASYMMETRIC
SALAMO-BASED DINUCLEAR NICKEL(II)
COMPLEX BEARING TWO DIFFERENT
COORDINATION MODES**

M. Li¹, L.-L. Li¹, P. Li¹, and W.-K. Dong^{1*}

An unprecedented dinuclear Ni(II) complex $[\{Ni_2(L)(HL)(\mu-OAc)(H_2O)\}_2] \cdot 3CH_3CH_2OH$ is successfully synthesized by the complexation of an asymmetric salamo-based ligand (H_2L) and Ni(II) acetate tetrahydrate and characterized by elemental analyses, UV-Vis and IR spectra, and X-ray crystallography analyses. Surprisingly, in the asymmetric unit of the Ni(II) complex, a fully deprotonated ligand (L^{2-}) unit and a partially deprotonated ligand (HL^-) unit wraps two Ni(II) atoms, with the $\mu-OAc^-$ anion bridging two adjacent Ni(II) atoms. The two Ni(II) atoms possess different coordination environments and twisted octahedral geometries. The hexacoordinated Ni(II) atom (Ni1) is located in the N_2O_4 donor cavity, but another hexacoordinated Ni(II) atom (Ni2) is located in a NO_5 donor coordination environment. Meanwhile, a 1D chain structure is formed by two $N-O \cdots \pi$ interactions. Hirshfeld surfaces and fluorescent properties are investigated.

DOI: 10.1134/S0022476622020093

Keywords: asymmetric salen-based ligand, Ni(II) complex, crystal structure, Hirshfeld surface analysis, fluorescent property.

INTRODUCTION

In recent years, considerable interest has been shown in the design and synthesis of polynuclear metal complexes from transition metal ions and organic ligands [1-3]. In particular, organometallic compounds containing N,O-donors have attracted much attention because of the potential use of these complexes in view of their remarkable biological activities [4, 5], prominent luminescent properties [8, 9], potential electrochemical properties [11, 12], as highly sensitive and selective fluorescent chemosensors [6, 7], excellent performance catalysts [10], and magnetic materials [13, 14]. Among them, salen-based N_2O_2 donor ligands with an alkyl ($-CH=N-C-X-C=N=CH-$) group [15, 16] have taken a significant share of the library of complexes over the last few decades throughout organic and inorganic chemistry, presumably due to their synthetic simplicity [17, 18].

Salamo-based ligand is a class of compounds with an O-alkyl oxime moiety ($-CH=N-O-(CH_2)_n-O-N=CH-$) developed by introducing the larger electronegativity of O atoms on the basis of a salen-based ligand [15, 19]. The stability of

¹School of Chemistry and Chemical Engineering, Lanzhou Jiaotong University, Lanzhou People's Republic of China; *dongwk@126.com. Original article submitted July 10, 2021; revised September 9, 2021; accepted September 10, 2021.

salamo-based ligands is greatly enhanced by the introduction of O atoms into the alkyl chain, and C=N bonds are not easy to suffer either exchange reaction or hydrolysis compared to salen-based ligands [20-23]. Owing to the ability of salamo-based ligands to react with transition metal ions to form a variety of metal complexes with novel homopolymeric [24, 25] and heteropolymeric [26-28] structures, this makes salamo-based ligands and their corresponding complexes have a great research value in the synthesis [29, 30], supramolecular structure [31-33], luminescence [34-37], and ion recognition [38-47] fields.

Here, a structurally unprecedented Ni(II) complex was prepared by the reaction of the asymmetric salamo-based ligand H₂L and Ni(II) acetate tetrahydrate. The complex has an unexpected dinuclear structure, and the structure has never been reported in the salamo-based Ni(II) complexes [48-50]. Thus, the structural diversity of the salamo-based complexes is further enriched.

EXPERIMENTAL

Materials and methods. 5-Nitrosalicylaldehyde (99%) and 3-methoxysalicylaldehyde (99%) were purchased from Alfa Aesar and used directly without further purification. Other reagents and solvents were analytical grade reagents from the Tianjin Chemical Reagent Factory.

The weight was weighed on a CP225D analytical balance manufactured by Sartorius, Germany.

Elemental analyses for the Ni(II) atom were conducted on an IRIS ER/S-WP-1 ICP atomic emission spectrometer. C, H, and N elemental analyses were performed on a GmbH Vario ELV3.00 automatic elemental analysis instrument.

Melting points were measured via a microscopic melting point apparatus made in Beijing Tektronix Instruments Limited Company, and the thermometer was uncorrected.

¹H NMR spectra were recorded on a Bruker AVANCE DRX-400 spectrometer (Bruker AVANCE, Billerica, MA, USA).

FTIR spectra were recorded on a VERTEX70 FTIR spectrophotometer, with samples prepared as KBr (4000-400 cm⁻¹) pellets.

UV-Vis absorption spectra were recorded on a Shimadzu UV-2550 spectrometer.

The X-ray single crystal structure was determined with a Bruker D8 Venture diffractometer.

The fluorescence spectra were measured by an F-7000 FL spectrophotometer.

Preparation of the H₂L ligand. The H₂L ligand was synthesized by following the method reported earlier [51].

Yield: 81%. M.p. 129.5-130.5 °C. Anal. calc. for C₁₇H₁₇N₃O₇ (%): C 54.40, H 4.57, N 11.20. Found (%): C 54.24, H 4.74, N 11.04. ¹H NMR (500 MHz, CDCl₃) δ 10.61 (s, 1H), 9.66 (s, 1H), 8.29 (s, 1H), 8.24 (s, 1H), 8.16 (dd, J = 9.0 Hz, 2.7 Hz, 1H), 8.13 (d, J = 2.7 Hz, 1H), 7.04 (d, J = 9.0 Hz, 1H), 6.91 (dd, J = 7.9, 1.16 Hz, 1H), 6.85 (dd, J = 10.0 Hz, 5.6 Hz, 1H), 6.81 (dd, J = 7.8 Hz, 1.6 Hz, 1H), 4.55-4.52 (m, 2H), 4.51-4.48 (m, 2H), 3.90 (s, 3H).

Synthesis of the Ni(II) complex. H₂L (3.75 mg, 0.01 mmol) was dissolved in 2 mL of CH₂Cl₂/CH₃CN (V/V = 1:1), and then 4 mL of an EtOH solution of Ni(II) acetate tetrahydrate (2.49 mg, 0.01 mmol) was added dropwise to the above solution at room temperature. The mixture was stirred for 10 min. A small quantity of the precipitate appeared during this process, which was filtered out and kept undisturbed to crystallize at room temperature with evaporating a part of the solution. Then green block-shaped single crystals suitable for the X-ray crystallographic analysis were obtained within a few days, collected by filtration, and air dried. Yield: 45%. Anal. calc. for [{Ni₂(L)(HL)(μ-OAc)(H₂O)}₂]·3CH₃CH₂OH (C₇₈H₉₀N₁₂Ni₄O₃₇) (%): C 46.32, H 4.49, N 8.31, Ni 11.61. Found (%): C 46.50, H 4.25, N 8.08, Ni 11.36.

X-ray structure determination of the Ni(II) complex. The crystal structure data for the Ni(II) complex was collected with graphite-monochromatized MoK_α radiation ($\lambda = 0.71073 \text{ \AA}$) at 173 K using the Bruker D8 Venture diffractometer. The complex structure was solved using SHELXT by intrinsic phasing [52]; the refinement was performed in Olex2 with SHELXL-2018 by the least-squares minimization against F^2 [53]. The non-hydrogen atoms were refined with anisotropic thermal parameters and the hydrogen atoms were refined with isotropic parameters. The data set was corrected for

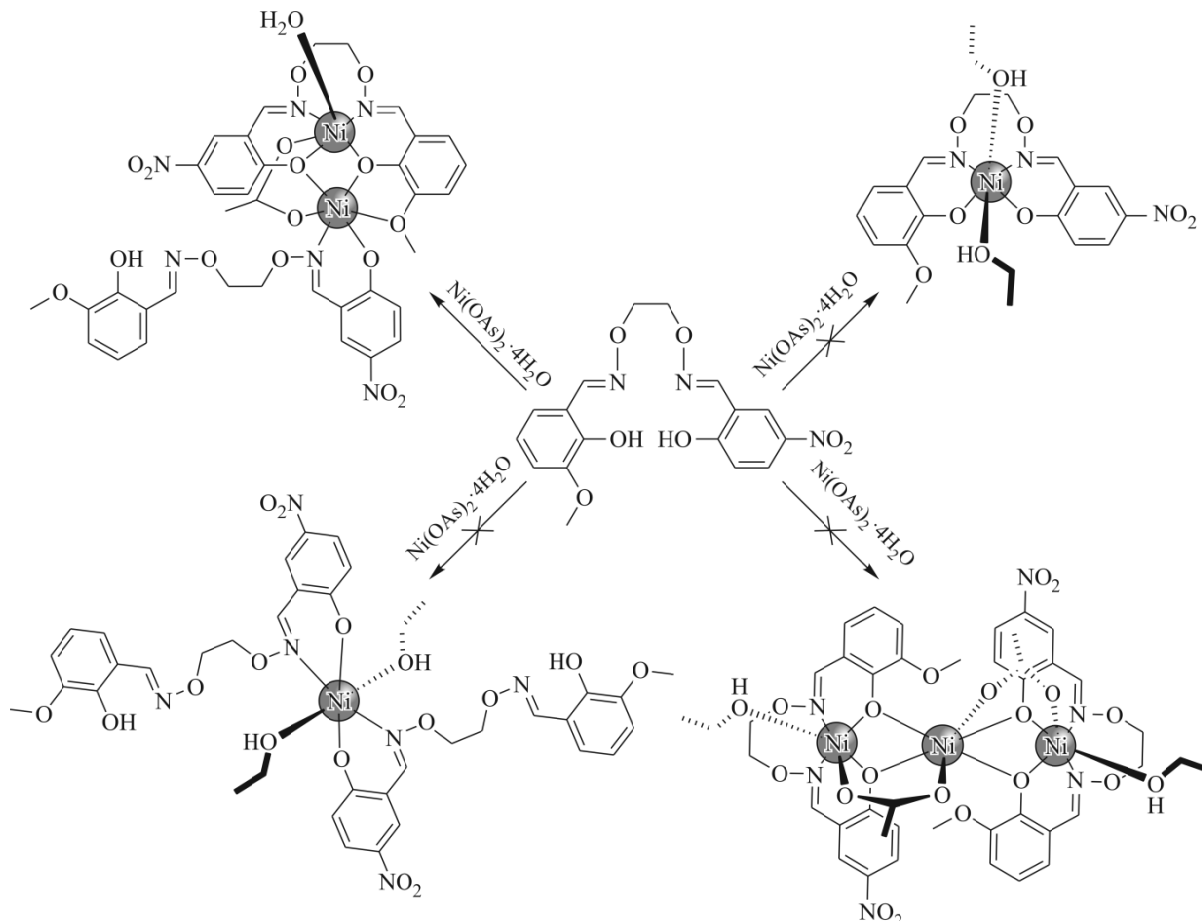
absorption based on multiple scans using the SADABS program [54]. Hydrogen atoms were placed in calculated positions and refined isotropically using a riding model.

The complete crystallographic data have been deposited as a CIF file with the Cambridge Crystallography Data Center (CCDC No. 2094835) and is available freely upon request citing the deposition number from the web site: <http://www.ccdc.cam.ac.uk/conts/retrieving.html>

The main crystallographic data are as follows: $C_{78}H_{90}N_{12}Ni_4O_{37}$, $M_r = 2022.45$, triclinic, $P\bar{1}$, space group, $a = 10.1044(4)$ Å, $b = 15.0972(6)$ Å, $c = 15.7916(7)$ Å, $\alpha = 67.2110(10)^\circ$, $\beta = 84.376(2)^\circ$, $\gamma = 89.306(2)^\circ$, $V = 2209.36(16)$ Å³ at $T = 173.0$ K, $Z = 1$, $d_x = 1.520$ g/cm³, $F_{000} = 1050.0$, $\mu = 0.936$ mm⁻¹, $-12 \leq h \leq 12$, $-19 \leq k \leq 19$, $-19 \leq l \leq 19$, $S = 0.996$, $R_1 = 0.0361$ for 8064 reflections with $I > 2\sigma(I)$, $wR_2 = 0.1167$ for all 9349 independent reflections.

RESULTS AND DISCUSSION

The synthetic route to $[\{\text{Ni}_2(\text{L})(\text{HL})(\mu\text{-OAc})(\text{H}_2\text{O})\}_2]\cdot 3\text{CH}_3\text{CH}_2\text{OH}$ is shown in Scheme 1. The reaction of the H₂L ligand with Ni(II) acetate tetrahydrate did not form the expected Ni(II) complexes [55-57].



Scheme 1. Synthetic route to the Ni(II) complex.

IR spectra. Various absorption peaks in the range of 4000–400 cm⁻¹ for the H₂L ligand and its corresponding Ni(II) complex are shown in Table 1 and Fig. 1.

The spectrum of H₂L showed two strong stretching vibrational bands at *ca.* 3429 cm⁻¹ and 3210 cm⁻¹, which indicates the presence of a multimolecular association and intramolecular hydrogen bonds $\nu(\text{O}-\text{H})$ [21, 58]. However, those of the corresponding Ni(II) complex showed a strong stretching vibration band and a shoulder peak at *ca.* 3419 cm⁻¹ and

TABLE 1. Major IR Spectral Data for H₂L and its Ni(II) Complex

Vibration bond	H ₂ L	Ni(II) complex	Vibration bond	H ₂ L	Ni(II) complex
$\nu(\text{O-H})$	3429	3419	$\nu(\text{C}=\text{N})$	1611	1608
	3210	3216		1575	1562
$\nu(\text{Ar-O})$	1260	1245	$\nu(\text{N}-\text{O})$	1260	1217
$\nu_{\text{as}}(\text{NO}_2)$	1521	1562	$\nu_{\text{s}}(\text{NO}_2)$	1353	1361
$\nu_{\text{as}}(\text{COO}^-)$	-	1562	$\nu_{\text{s}}(\text{COO}^-)$	-	1470
$\nu(M-\text{O})$	-	477	$\nu(M-\text{N})$	-	523

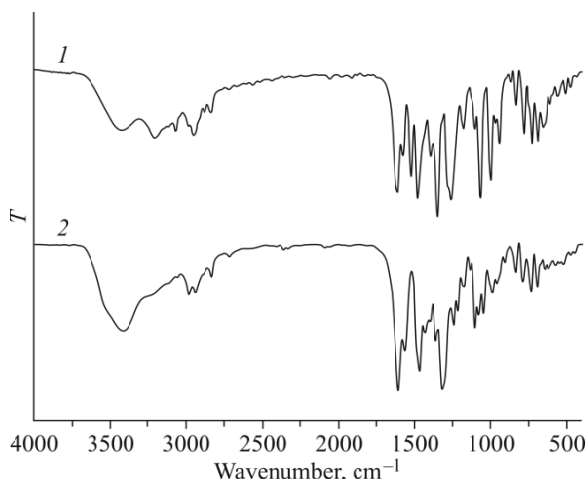


Fig. 1. IR spectra of the H₂L (1) ligand and its corresponding Ni(II) complex (2).

3216 cm⁻¹, respectively, reflecting that the Ni(II) complex contained partially deprotonated OH groups of the H₂L ligand, water, and ethanol molecules [24, 40, 59]. This result is in agreement with the elemental analysis result mentioned above. The C=N stretching vibration and the carbon skeleton bands of benzene rings for the H₂L ligand and its corresponding Ni(II) complex were shifted towards lower wavenumbers due to the conjugation of C=N groups with the benzene rings. The H₂L ligand showed a characteristic C=N stretching vibrational band [56] and the carbon skeleton band of the benzene rings [60] at *ca.* 1611 cm⁻¹ and 1575 cm⁻¹, respectively. Compared with the free ligand, the characteristic absorption of the corresponding positions of the Ni(II) complex were red-shifted to *ca.* 1608 cm⁻¹ and 1562 cm⁻¹. The N–O stretching vibration from –C=N–O–C– fragments in the H₂L ligand were superimposed on the Ar–O vibrational bands and appeared at *ca.* 1260 cm⁻¹ due to the close frequency, while the N–O and Ar–O stretching vibrational bands for the Ni(II) complex emerged at *ca.* 1217 cm⁻¹ and 1245 cm⁻¹, respectively. In the H₂L ligand, the bands at *ca.* 1521 cm⁻¹ and 1353 cm⁻¹ can be attributed to the asymmetric (ν_{as}) and symmetric (ν_{s}) stretching vibrational bands of the NO₂ group, respectively [61]. The bands associated with the symmetric stretching vibration $\nu_{\text{s}}(\text{NO}_2)$ occurred at *ca.* 1361 cm⁻¹ for the Ni(II) complex, while the asymmetric stretching vibration of NO₂ and OAc⁻ groups ($\nu_{\text{as}}(\text{NO}_2)$ and $\nu_{\text{as}}(\text{COO}^-)$) for the Ni(II) complex overlapped at *ca.* 1562 cm⁻¹ due to the close frequency. The symmetric stretching vibration $\nu_{\text{s}}(\text{COO}^-)$ of OAc⁻ in the Ni(II) complex appeared at 1470 cm⁻¹. These data confirmed that the H₂L ligand and OAc⁻ are coordinated to Ni(II) atoms, and Ni–N and Ni–O bonds are formed by Ni(II) atoms coordinated with nitrogen atoms of the C=N groups, oxygen atoms of Ar–O and the OAc⁻ group [56, 62].

It is well known that carboxylate can be coordinated with metal ions in a bidentate or monodentate manner. The Δ criterion is based on the difference between the $\nu_{\text{as}}(\text{COO}^-)$ and $\nu_{\text{s}}(\text{COO}^-)$ values and the corresponding values in sodium acetate and is currently used to determine the coordination pattern of acetate [63]. The value $\Delta\nu = 92 \text{ cm}^{-1}$ indicates that the acetate group in the Ni(II) complex acts as a bidentate ligand [63].

The far-IR spectrum of the Ni(II) complex was gained in order to distinguish frequencies due to the Ni–O and Ni–N bonds. The stretching vibrational bands exhibit Ni–O and Ni–N vibrational absorption frequencies at *ca.* 477 cm⁻¹ and 523 cm⁻¹, indicating that Ni(II) atoms are coordinated with N- and O-donor atoms of the H₂L ligand [64].

UV-Vis absorption spectra. As depicted in Fig. 2, the UV-Vis spectra of H₂L and its correspondding Ni(II) complex in ethanol (2·10⁻⁵ M) possess various absorption peaks in the range of 245–500 nm. The strong absorption peak corresponding to $\pi-\pi^*$ transitions of the benzene rings was observed in the free H₂L ligand at about 270 nm [65, 66]. There is an obvious absorption peak in the spectrum of the free H₂L ligand at about 310 nm, which is assigned to the $\pi-\pi^*$ transition of C=N bonds [64]. The $\pi-\pi^*$ transitions occurring in benzene rings underwent a bathochromic shift in the corresponding Ni(II) complex and appeared at about 275 nm. Meanwhile, the absorption peak at 310 nm in the UV-Vis spectrum of the Ni(II) complex disappeared, compared to that of the free H₂L ligand, suggesting that the oxime nitrogen atoms were involved in the coordination to Ni(II) atoms. In addition, a new absorption peak appeared at about 370 nm, which belonged to the $n-\pi^*$ charge transfer from the N lone pairs of C=N groups to the ligand [24].

The ethanol solution of Ni²⁺ ions (2·10⁻³ M) was gradually added to an ethanol solution of H₂L. The corresponding peak at about 270 nm is bathochromically shifted to 275 nm, which indicates the coordination of Ni²⁺ ions. The absorption peak at about 310 nm disappeared, and a new absorption peak appeared at about 370 nm, and two isoabsorbance points appeared at about 226 nm and 331 nm. When one equivalent of Ni²⁺ ions was added, the absorption spectra no longer changed (Fig. 3), indicating that the optimal combination of H₂L and Ni²⁺ is 1:1 and it was consistent with the X-ray crystallographic analysis [26].

Crystal structure description. The main bond lengths and bond angles of the Ni(II) complex are listed in Table 2.

The Ni(II) complex crystallizes in the triclinic system with the space group $P\bar{1}$. The X-ray structure analysis shows that the Ni(II) complex is an unprecedented 1:1:2 ((L)²⁻:(HL)⁻:Ni²⁺) dinuclear structure which is entirely different from the structures of 1:1 [55], 2:1 [56], and 2:3 [57] ((L)²⁻:Ni²⁺ or (HL)⁻:Ni²⁺) reported previously in the salamo-based Ni(II) complexes. The formula of the Ni(II) complex is $[\{\text{Ni}_2(\text{L})(\text{HL})(\mu\text{-OAc})(\text{H}_2\text{O})\}_2]\cdot 3\text{CH}_3\text{CH}_2\text{OH}$. The crystal structure and main atomic labels of the Ni(II) complex are shown in Fig. 4.

The Ni(II) complex includes two Ni(II) atoms, one fully deprotonated ligand (L)²⁻ unit, one partially deprotonated ligand (HL)⁻ unit, one $\mu\text{-OAc}^-$ anion, one coordinated water molecule, and one and half crystallized ethanol molecules, as expected from the results of the elemental analysis. In the asymmetric unit of the Ni(II) complex, the central hexacoordinated Ni(II) atom (Ni1) is located in the N₂O₂ cavity of the fully deprotonated ligand (L)²⁻ unit; the equatorial sites around the Ni1 atom are occupied by donor atoms (N₂, N₃, O₃, and O₆) of the ligand (L)²⁻ unit; two axial positions are occupied by the oxygen atom (O₁₇) of the $\mu\text{-OAc}^-$ anion and the oxygen atom (O₁₅) of the coordinated water molecule (Fig. 4a), forming

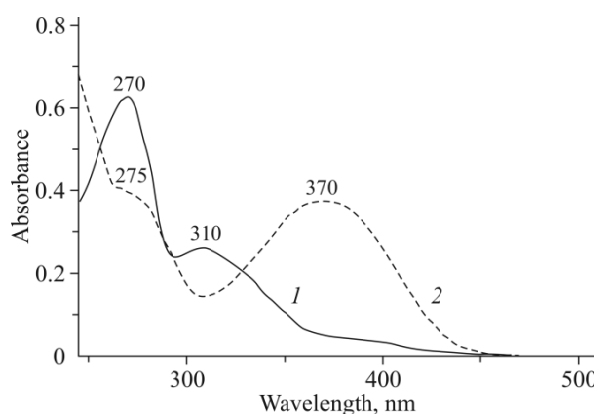


Fig. 2. UV-Vis absorption spectra of the H₂L ligand (1) and its corresponding Ni(II) complex (2) in EtOH (2·10⁻⁵ M).

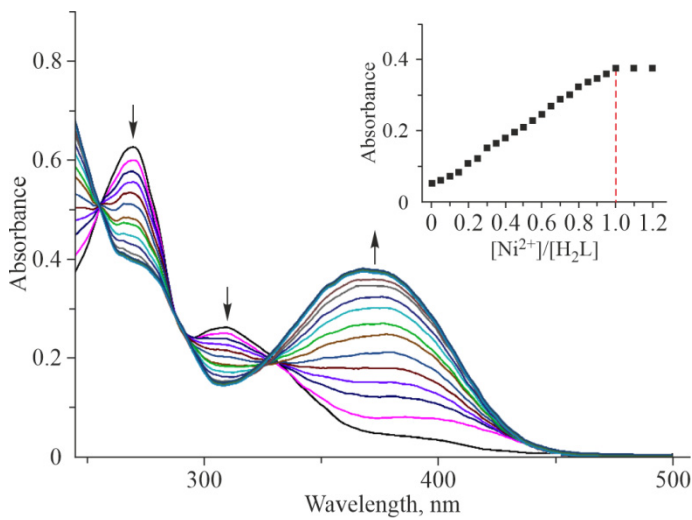


Fig. 3. UV-Vis titration spectral changes of the Ni(II) complex; inset: absorbance at 370 nm varies with the interaction of $[Ni^{2+}]/[H_2L]$.

TABLE 2. Selected Bond Lengths and Bond Angles for the Ni(II) Complex

Bond length	Distance, Å	Bond length	Distance, Å
Ni1–O3	2.0501(16)	Ni2–O3	2.0600(16)
Ni1–O6	2.0176(17)	Ni2–O6	2.0077(16)
Ni1–O15	2.0823(16)	Ni2–O7	2.1964(19)
Ni1–O17	2.0328(16)	Ni2–O10	2.0116(16)
Ni1–N2	2.105(2)	Ni2–O16	2.0266(16)
Ni1–N3	2.118(2)	Ni2–N5	2.035(2)
Bond angle	Value, deg	Bond angle	Value, deg
O3–Ni1–O6	80.11(7)	O3–Ni2–O6	80.10(7)
O3–Ni1–O15	91.12(6)	O3–Ni2–O7	86.9(2)
O3–Ni1–O17	92.28(6)	O3–Ni2–O10	96.44(7)
O3–Ni1–N2	85.75(7)	O3–Ni2–O16	91.03(7)
O3–Ni1–N3	165.81(8)	O3–Ni2–N5	104.03(8)
O6–Ni1–O15	89.46(6)	O6–Ni2–O7	77.87(6)
O6–Ni1–O17	91.83(6)	O6–Ni2–O10	91.82(7)
O6–Ni1–N2	165.80(7)	O6–Ni2–O16	88.64(6)
O6–Ni1–N3	85.90(7)	O6–Ni2–N5	175.86(8)
O15–Ni1–O17	176.52(6)	O7–Ni2–O10	88.05(7)
O3–Ni1–O6	80.11(7)	O7–Ni2–O16	84.71(7)
O3–Ni1–O15	91.12(6)	O7–Ni2–N5	98.00(7)
O3–Ni1–O17	92.28(6)	O10–Ni2–O16	172.48(7)
O15–Ni1–N2	89.56(7)	O10–Ni2–N5	88.04(7)
O15–Ni1–N3	86.39(7)	O16–Ni2–N5	90.96(7)
O17–Ni1–N2	89.98(7)	O6–Ni2–O7	77.87(6)
O17–Ni1–N3	90.48(7)	O6–Ni2–O10	91.82(7)
N2–Ni1–N3	108.17(8)	O6–Ni2–O16	88.64(6)

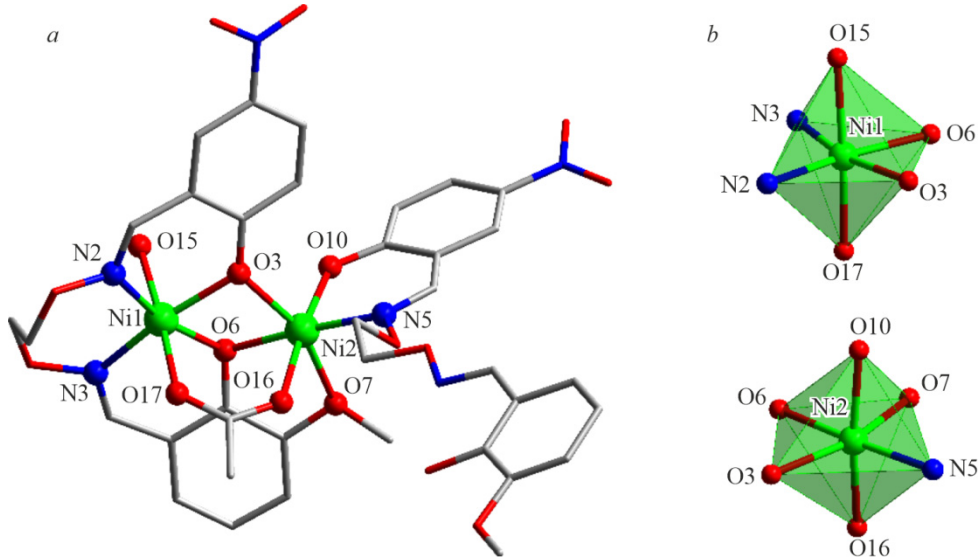


Fig. 4. X-ray crystal structure of the Ni(II) complex; hydrogen atoms and solvent molecules are omitted for clarity (*a*); coordination configurations of Ni(II) atoms in the Ni(II) complex (*b*).

a twisted octahedral geometry (Fig. 4*b*). Meanwhile, another hexacoordinated Ni(II) atom (Ni2) is not located in the N_2O_2 cavity of the ligand (HL^-) unit and is surrounded by two phenolic oxygen atoms (O3 and O6) from the ligand (L^{2-}) unit, one methoxy oxygen atom (O7), one oxygen atom (O16) from the $\mu\text{-OAc}^-$ anion, one oxime nitrogen atom (N5), and one phenolic oxygen atom (O10) from the partially deprotonated (HL^-) unit. Four atoms (N5, O3, O6, and O7) form a equatorial plane; two oxygen atoms (O10 and O16) occupy the axial positions, adopting a twisted octahedral geometry (Fig. 4*b*).

In the structure of the Ni(II) complex there are five pairs of intramolecular hydrogen bonds (C25–H25B…O16, C8–H8B…O17, C8–H8B…N3, C9–H9B…N2, and O13–H13…N6), which are shown in Fig. 5.

Finally, a 2D supramolecular structure is formed by five pairs of intermolecular hydrogen bonding interactions (O15–H15A…O2, O15–H15B…O18, O18–H18…O10, C3–H3…O8, and C16–H16…O18) in the Ni(II) complex, as shown in Fig. 6. The intramolecular and intermolecular hydrogen bonds are the basis of the stable supramolecular structure and are listed in Table 3.

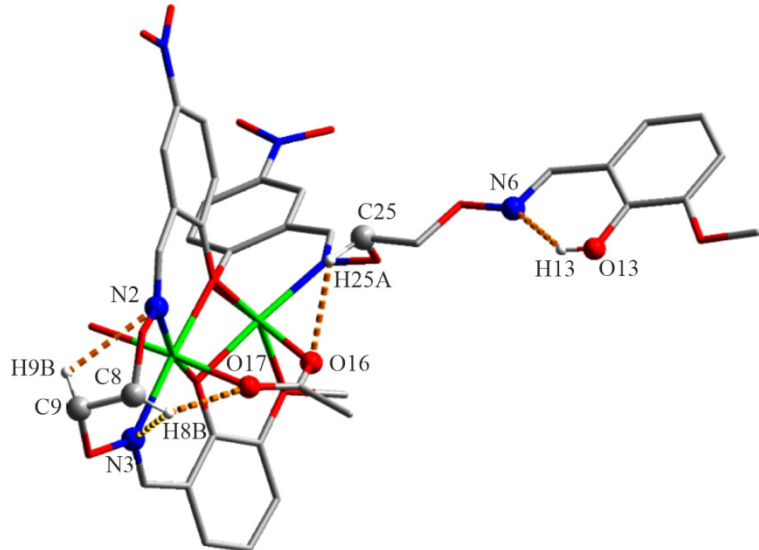


Fig. 5. View of intramolecular hydrogen bonds of the Ni(II) complex.

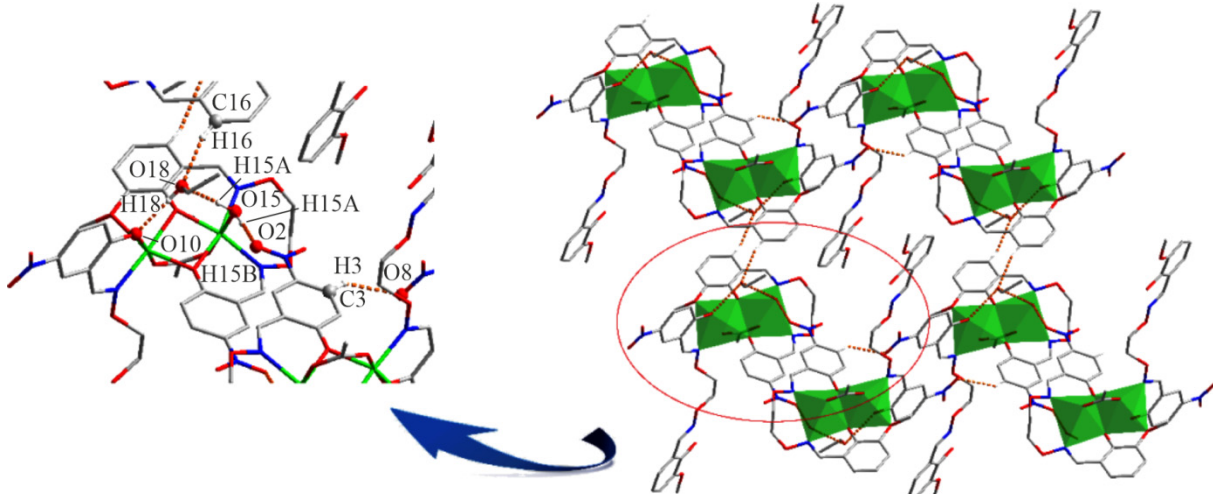


Fig. 6. 2D supramolecular structure with intermolecular hydrogen bonding interactions in the Ni(II) complex, which are indicated by dashed lines; hydrogen atoms, except those forming hydrogen bonds, are omitted for clarity.

TABLE 3. Intermolecular Hydrogen Bonding Interactions of the Ni(II) Complex

$D\text{-H}\cdots A$	$d_{(D\text{-H})}, \text{\AA}$	$d_{(H\text{-}A)}, \text{\AA}$	$d_{(D\text{-}A)}, \text{\AA}$	$\angle(D\text{HA}), \text{deg}$	Symmetry code
O13-H13···N6	0.84	1.92	2.648(3)	144	
O15-H15A···O2	0.84	2.08	2.906(3)	168	$-x, 1-y, 2-z$
O15-H15B···O18	0.84	1.87	2.707(3)	176	
O18-H18···O10	0.84	1.93	2.762(3)	174	
C3-H3···O8	0.95	2.44	3.204(3)	137	$-x, 1-y, 1-z$
C8-H8B···O17	0.99	2.55	3.365(3)	140	
C8-H8B···N3	0.99	2.50	2.895(4)	103	
C9-H9B···N2	0.99	2.51	2.900(3)	103	
C16-H16···O18	0.95	2.45	3.378(4)	165	$1-x, -y, 2-z$
C25-H25B···O16	0.99	2.47	3.086(3)	120	

Two N–O··· π (N1–O2···Cg1 and N4–O8···Cg2 (Cg1: C1–C2–C3–C4–C5–C6; Cg2: C18–C19–C20–C21–C22–C23)) interactions are found in the Ni(II) complex. Fig. 7 shows a 1D chain structure organized by N–O··· π interactions in the Ni(II) complex.

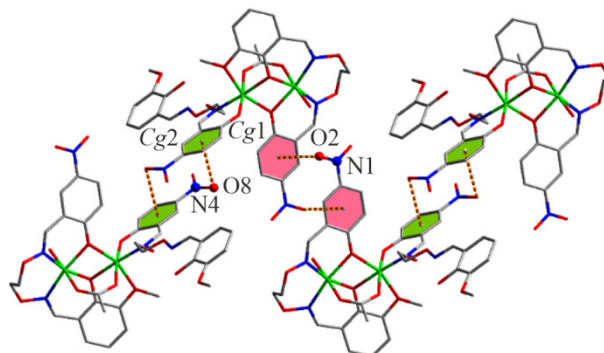


Fig. 7. N–O··· π interactions of the Ni(II) complex; hydrogen atoms and solvent molecules are omitted for clarity.

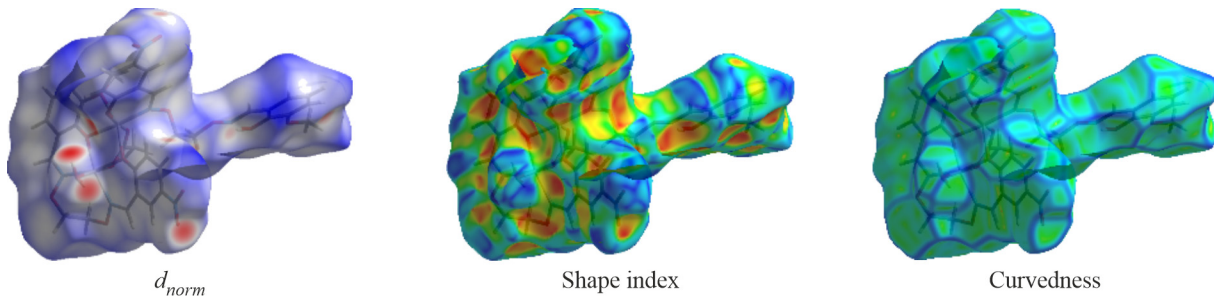


Fig. 8. Hirshfeld surface analysis map of the Ni(II) complex.

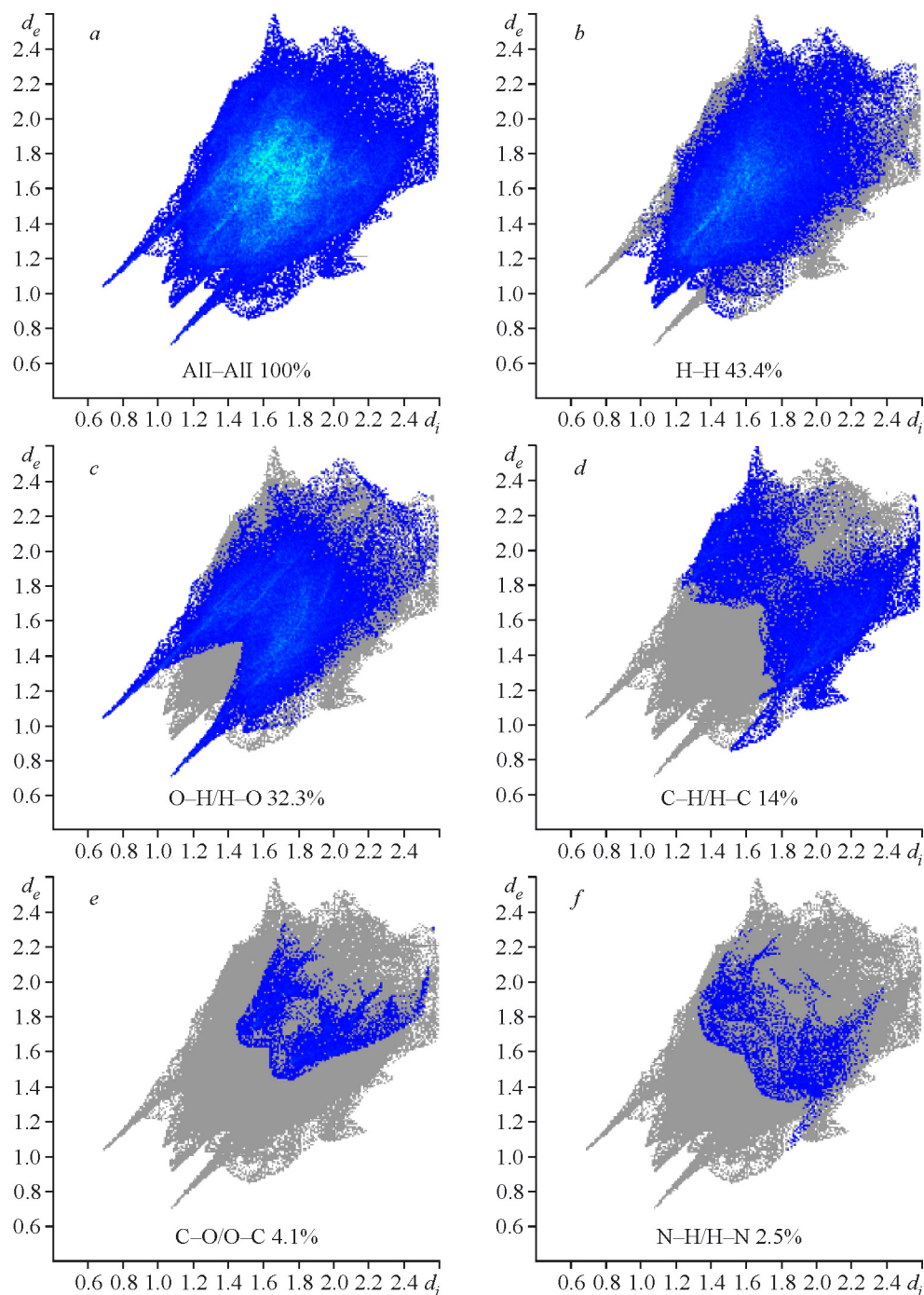


Fig. 9. 2D FP for various molecular interactions of the Ni(II) complex.

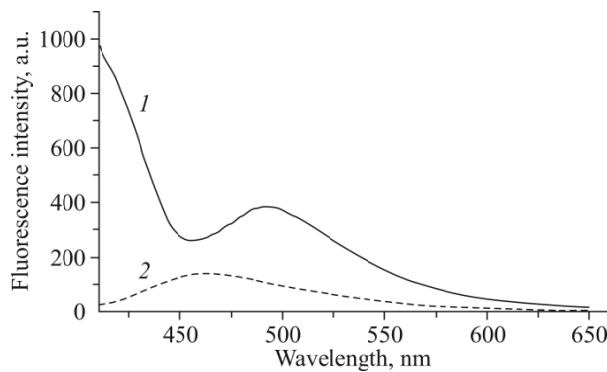


Fig. 10. Fluorescence spectra of H_2L (1) and its correspondding Ni(II) complex (2).

Hirshfeld surface analysis. The Hirshfeld surface analysis [67] was carried out by selecting the asymmetric unit among the entire unit cell of the Ni(II) complex. The surfaces are shown as transparent to allow visualization of the molecular moiety (Fig. 8), showing surfaces mapped over d_{norm} , a shape index and curvedness.

The large deep red circular depressions visible on the d_{norm} surfaces are indicative of hydrogen bonding interactions in the Ni(II) complex, and other visible spots are due to H–H interactions. The small extent of the area and light color on the surface indicates weaker and longer interactions other than hydrogen bonds. The clear blue lines correspond to lone pair interactions in the Ni(II) complex molecules [31].

Fig. 9 illustrates the breakdown of 2D fingerprint plots (FPs) of the Hirshfeld surface for the Ni(II) complex. The blue area represents the proportion of each short-range effect and gray represents the entire fingerprint [68]. With these analyses, the division of contributions is possible for different interactions, including H–H, O–H, C–H, C–O, N–H, which commonly overlap in entire FPs. The predominant interaction in the Ni(II) complex is the H–H interaction, which accounts for 43.4%. The next most important interactions are O–H/H–O, contributing 32.3%. Taking these interactions as an example, the H–O interaction is mainly concentrated in the peak position at the upper left of the fingerprint, while the O–H interaction is mainly concentrated in the peak position at the lower right of the fingerprint. The other strong interactions are C–H/H–C interactions which contribute 14% to the complex molecule. The other significant interactions are C–O/O–C and N–H/H–N, which account for 4.1% and 2.5%, respectively. All these interactions are responsible for the stability of the molecules of the Ni(II) complex.

Fluorescent properties. The fluorescence spectra of H_2L and its corresponding Ni(II) complex were obtained at an excitation wavelength of 375 nm in a DMF solution ($5 \cdot 10^{-5}$ M), which is depicted in Fig. 10.

A broad emission band and stronger fluorescence at an approximately 490 nm emission wavelength can be assigned to the $\pi-\pi^*$ charge transition in the H_2L molecule [64]. Under the same conditions, the maximum emission band of the Ni(II) complex has a blue shift to approximately 463 nm relative to H_2L , showing fluorescence quenching, which may be caused by the ligand-to-metal charge transfer (LMCT) [37, 46].

CONCLUSIONS

A unprecedented Ni(II) complex $[\{\text{Ni}_2(\text{L})(\text{HL})(\mu\text{-OAc})(\text{H}_2\text{O})\}_2]\cdot\text{CH}_3\text{CH}_2\text{OH}$ was successfully prepared using an asymmetric salamo-based ligand H_2L and Ni(II) acetate tetrahydrate, and its structure was characterized by the X-ray structure determination. In the asymmetric unit of the Ni(II) complex, two Ni(II) atoms are surrounded by the fully deprotonated ligand (L^{2-}) unit and the partially deprotonated ligand (HL^-) unit, respectively. Both hexacoordinated Ni(II) atoms possess twisted octahedral configurations. Furthermore, two N–O \cdots π interactions exist in the Ni(II) complex, which leads to a 1D chain structure. The presence of various interactions in the Ni(II) complex was analyzed by the Hirshfeld

surface analysis. The Ni(II) complex has a blue shift with the maximum emission band and quenched fluorescence, as compared to the ligand, which is caused by LMCT when excited at 375 nm.

FUNDING

This work was supported by the National Natural Science Foundation of China (21761018), which is gratefully acknowledged.

CONFLICT OF INTERESTS

The authors declare that they have no conflict of interests.

REFERENCES

1. M. Eddaoudi, D. B. Moler, H. Li, B. Chen, T. M. Reineke, M. O'Keeffe, and O. M. Yaghi. *Acc. Chem. Res.*, **2001**, *34*, 319-330. <https://doi.org/10.1021/ar000034b>
2. P. Zanello, S. Tamburini, P. A. Vigato, and G. A. Mazzocchin. *Coord. Chem. Rev.*, **1987**, *77*, 165-273. [https://doi.org/10.1016/0010-8545\(87\)85034-8](https://doi.org/10.1016/0010-8545(87)85034-8)
3. P. A. Vigato and S. Tamburini. *Coord. Chem. Rev.*, **2004**, *248*, 1717-2128. <https://doi.org/10.1016/j.cct.2003.09.003>
4. E. Yousif, A. Majeed, K. A. Sammarrae, N. Salih, J. Salimon, and B. Abdullah. *Arab. J. Chem.*, **2017**, *10*, 1639-1644. <https://doi.org/10.1016/j.arabjc.2013.06.006>
5. B. K. Kundu, Pragti, S. M. Mobin, and S. Mukhopadhyay. *Dalton Trans.*, **2020**, *49*, 15481-15503. <https://doi.org/10.1039/D0DT02941F>
6. M. Shyamal, P. Mazumdar, S. Maity, S. Samanta, G. P. Sahoo, and A. Misra. *ACS Sens.*, **2016**, *1*(6), 739-747. <https://doi.org/10.1021/acssensors.6b00289>
7. Y. Wu, W. M. Ding, J. Li, G. Guo, S. Z. Zhang, H. R. Jia, and Y. X. Sun. *J. Fluoresc.*, **2021**, *31*, 437-446. <https://doi.org/10.1007/s10895-020-02677-x>
8. J. Andrez, V. Guidal, R. Scopelliti, J. Pecaut, S. Gambarelli, and M. Mazzanti. *J. Am. Chem. Soc.*, **2017**, *139*, 8628-8638. <https://doi.org/10.1021/jacs.7b03604>
9. S. Z. Zhang, G. Guo, W. M. Ding, J. Li, Y. Wu, H. J. Zhang, J. Q. Guo, and Y. X. Sun. *J. Mol. Struct.*, **2021**, *1230*(12), 129627. <https://doi.org/10.1016/j.molstruc.2020.129627>
10. M. Jafarian, M. Rashvand avei, M. Khakali, F. Gobal, S. Rayati, and M. G. Mahjani. *J. Phys. Chem. C*, **2012**, *116*, 18518-18532. <https://doi.org/10.1021/jp305370m>
11. B. E. Klamm, C. J. Windorff, C. C. Barros, M. L. Marsh, and T. E. A. Schmitt. *Inorg. Chem.*, **2020**, *59*(1), 23-31. <https://doi.org/10.1021/acs.inorgchem.9b00477>
12. M. Chakraborty, A. Mondal, and S. K. Chattopadhyay. *New J. Chem.*, **2020**, *44*, 12916-12925. <https://doi.org/10.1039/D0NJ00719F>
13. L. K. Das, A. Biswas, C. J. G. Garćía, M. G. B. Drew, and A. Ghosh. *Inorg. Chem.*, **2014**, *53*(1), 434-445. <https://doi.org/10.1021/ic402415b>
14. A. Bhanja, R. Herchel, Z. Trávníček, and D. Ray. *Inorg. Chem.*, **2019**, *58*(18), 12184-12198. <https://doi.org/10.1021/acs.inorgchem.9b01517>
15. S. Akine, T. Taniguchi, and T. Nabeshima. *Chem. Lett.*, **2001**, *30*(7), 682/683. <https://doi.org/10.1246/cl.2001.682>
16. T. Feng, L. L. Li, Y. J. Li, and W. K. Dong. *Acta Crystallogr., Sect. B*, **2021**, *77*, 168-181. <https://doi.org/10.1107/S2052520620016157>
17. E. Sinn and C. M. Harris. *Coord. Chem. Rev.*, **1969**, *4*(4), 391-422. [https://doi.org/10.1016/S0010-8545\(00\)80080-6](https://doi.org/10.1016/S0010-8545(00)80080-6)

18. S. Akine and T. Nabeshima. *Dalton Trans.*, **2009**, *47*, 10395-10408. <https://doi.org/10.1039/b910989g>
19. R. N. Bian, J. F. Wang, X. Xu, X. Y. Dong, and Y. J. Ding. *Appl. Organomet. Chem.*, **2021**, *35*, e6040. <https://doi.org/10.1002/aoc.6040>
20. S. Akine and T. Nabeshima. *Inorg. Chem.*, **2005**, *44*, 1205-1207. <https://doi.org/10.1021/ic048347g>
21. Y. D. Peng, R. Y. Li, P. Li, and Y. X. Sun. *Crystals*, **2021**, *11*, 113. <https://doi.org/10.3390/crust11020113>
22. X. Xu, Y. J. Li, T. Feng, W. K. Dong, and Y. J. Ding. *Luminescence*, **2021**, *36*, 169-179. <https://doi.org/10.1002/bio.3932>
23. C. Liu, Z. L. Wei, H. R. Mu, W. K. Dong, and Y. J. Ding. *J. Photochem. Photobiol. A*, **2020**, *397*, 112569. <https://doi.org/10.1016/j.jphotochem.2020.112569>
24. P. Li, G. X. Yao, M. Li, and W. K. Dong. *Polyhedron*, **2021**, *195*, 114981. <https://doi.org/10.1016/j.poly.2020.114981>
25. M. Yu, Y. Zhang, Y. Q. Pan, and L. Wang. *Inorg. Chim. Acta*, **2020**, *509*, 119701. <https://doi.org/10.1016/j.ica.2020.119701>
26. C. Liu, X. X. An, Y. F. Cui, K. F. Xie, and W. K. Dong. *Appl. Organometal. Chem.*, **2020**, *34*, e5272. <https://doi.org/10.1002/aoc.5272>
27. Y. F. Cui, C. Liu, Y. Zhang, and Y. Zhang. *Inorg. Nano-Met. Chem.*, **2021**, *51*(2), 288-295. <https://doi.org/10.1080/24701556.2020.1776735>
28. X. X. An, Z. Z. Chen, H. R. Mu, and L. Zhao. *Inorg. Chim. Acta*, **2020**, *511*, 119823. <https://doi.org/10.1016/j.ica.2020.119823>
29. S. Akine, T. Taniguchi, and T. Nabeshima. *J. Am. Chem. Soc.*, **2006**, *128*, 15765-15774. <https://doi.org/10.1021/ja0646702>
30. S. Akine, T. Tadokoro, and T. Nabeshima. *Inorg. Chem.*, **2012**, *51*, 11478-11486. <https://doi.org/10.1021/ic3012525>
31. J. F. Wang, T. Feng, Y. J. Li, Y. X. Sun, W. K. Dong, and Y. J. Ding. *J. Mol. Struct.*, **2021**, *1231*, 129950. <https://doi.org/10.1016/j.molstruc.2021.129950>
32. J. F. Wang, X. Xu, R. N. Bian, W. K. Dong, and Y. J. Ding. *Inorg. Chim. Acta*, **2021**, *516*, 120095. <https://doi.org/10.1016/j.ica.2020.120095>
33. Y. X. Sun, Y. Q. Pan, X. Xu, and Y. Zhang. *Crystals* **2019**, *9*, 607. <https://doi.org/10.3390/crust9120607>
34. L. W. Zhang, Y. Zhang, Y. F. Cui, M. Yu, and W. K. Dong. *Inorg. Chim. Acta*, **2020**, *506*, 119534. <https://doi.org/10.1016/j.ica.2020.119534>
35. Q. P. Kang, X. Y. Li, Z. L. Wei, Y. Zhang, and W. K. Dong. *Polyhedron*, **2019**, *165*, 38-50. <https://doi.org/10.1016/j.poly.2019.03.008>
36. Q. P. Kang, X. Y. Li, L. Wang, Y. Zhang, and W. K. Dong. *Appl. Organomet. Chem.*, **2019**, *33*, e5013. <https://doi.org/10.1002/aoc.5013>
37. Q. Zhao, X. X. An, L. Z. Liu, and W. K. Dong. *Inorg. Chim. Acta*, **2019**, *490*, 6-15. <https://doi.org/10.1016/j.ica.2019.02.040>
38. J. F. Wang, R. N. Bian, T. Feng, K. F. Xie, L. Wang, and Y. J. Ding. *Microchem. J.*, **2021**, *160*, 105676. <https://doi.org/10.1016/j.microc.2020.105676>
39. R. N. Bian, X. Xu, T. Feng, and W. K. Dong. *Inorg. Chim. Acta*, **2021**, *516*, 120098. <https://doi.org/10.1016/j.ica.2020.120098>
40. H. R. Mu, M. Yu, L. Wang, Y. Zhang, and W. K. Dong. *Phosphorus, Sulfur Silicon Relat. Elem.*, **2020**, *195*(9), 730-739. <https://doi.org/10.1080/10426507.2020.1756807>
41. L. Wang, Z. L. Wei, C. Liu, W. K. Dong, and J. X. Ru. *Spectrochim. Acta, Part A*, **2020**, *239*, 118496. <https://doi.org/10.1016/j.saa.2020.118496>
42. L. Wang, Z. L. Wei, Z. Z. Chen, C. Liu, W. K. Dong, and Y. J. Ding. *Microchem. J.*, **2020**, *155*, 104801. <https://doi.org/10.1016/j.microc.2020.104801>

43. R. Y. Li, Z. L. Wei, L. Wang, Y. Zhang, and J. X. Ru. *Spectrochim. Acta, Part A*, **2020**, 228, 117775. <https://doi.org/10.1016/j.saa.2019.117775>
44. Z. L. Wei, L. Wang, J. F. Wang, W. T. Guo, Y. Zhang, and W. K. Dong. *Spectrochim. Acta, Part A*, **2020**, 228, 117775. <https://doi.org/10.1016/j.saa.2019.117775>
45. Y. Q. Pan, X. Xu, Y. Zhang, Y. Zhang, and W. K. Dong. *Spectrochim. Acta, Part A*, **2020**, 229, 117927. <https://doi.org/10.1016/j.saa.2019.117927>
46. L. Wang, Y. Q. Pan, J. F. Wang, Y. Zhang, and Y. J. Ding. *J. Photochem. Photobiol. A*, **2020**, 400, 112719. <https://doi.org/10.1016/j.jphotochem.2020.112719>
47. L. Z. Liu, L. Wang, M. Yu, Q. Zhao, Y. Zhang, Y. X. Sun, and W. K. Dong. *Spectrochim. Acta, Part A*, **2019**, 222, 117209. <https://doi.org/10.1016/j.saa.2019.117209>
48. X. Xu, T. Feng, S. S. Feng, and W. K. Dong. *Appl. Organomet. Chem.*, **2021**, 35, e6057. <https://doi.org/10.1002/aoc.6057>
49. X. X. An, Q. Zhao, H. R. Mu, and W. K. Dong. *Crystals*, **2019**, 9, 101. <https://doi.org/10.3390/crust9020101>
50. Y. J. Li, S. Z. Guo, T. Feng, K. F. Xie, and W. K. Dong. *J. Mol. Struct.*, **2021**, 1228, 129796. <https://doi.org/10.1016/j.molstruc.2020.129796>
51. W. K. Dong, Y. X. Sun, S. J. Xing, Y. Wang, and X. H. Gao. *Z. Naturforsch. B: J. Chem. Sci.*, **2012**, 67, 197-203. <https://doi.org/10.1515/znb-2012-0303>
52. G. M. Sheldrick. *Acta Crystallor., Sect. A*, **2015**, 71, 3-8. <https://doi.org/10.1107/S2053273314026370>
53. G. M. Sheldrick. *Acta Crystallor., Sect. C*, **2015**, 71, 3-8. <https://doi.org/10.1107/S2053229614024218>
54. L. Krause, R. H. Irmer, G. M. Sheldrick, and D. Stalke. *J. Appl. Crystallogr.*, **2015**, 48, 3-10. <https://doi.org/10.1107/S1600576714022985>
55. S. Akine and T. Nabeshima. *Inorg. Chem.*, **2005**, 44, 1205-1207. <https://doi.org/10.1021/ic048347g>
56. W. K. Dong, L. C. Zhu, J. C. Ma, Y. X. Sun, and Y. Zhang. *Inorg. Chim. Acta*, **2016**, 453, 402-408. <https://doi.org/10.1016/j.ica.2016.08.050>
57. Y. Zhang, L. Z. Liu, Y. D. Peng, N. Li, and W. K. Dong. *Transit. Met. Chem.*, **2019**, 44, 627-639. <https://doi.org/10.1007/s11243-019-00325-3>
58. Y. Q. Pan, Y. Zhang, M. Yu, Y. Zhang, and L. Wang. *Appl. Organomet. Chem.*, **2020**, 34, e5441. <https://doi.org/10.1002/aoc.5441>
59. M. G. B. Drew, A. H. Othman, S. G. McFall, P. D. A. McIlroy, and S. M. Nelson. *J. Chem. Soc., Dalton Trans.*, **1977**, 438-446. <https://doi.org/10.1039/DT9770000438>
60. N. B. Colthu. *J. Opt. Soc. Am.*, **1950**, 40(6), 397-400. <https://doi.org/10.1364/JOSA.40.000397>
61. J. F. Brown. *J. Am. Ceram. Soc.*, **1955**, 77(23), 6341-6351. <https://doi.org/10.1021/ja01628a078>
62. X. Y. Li, Q. P. Kang, C. Liu, Y. Zhang, and W. K. Dong. *New J. Chem.*, **2019**, 43, 4605. <https://doi.org/10.1039/C9NJ00014C>
63. S. Musumeci, E. Rizzarelli, S. Sammartano, and A. Seminara. *Z. Anorg. Allg. Chem.*, **1977**, 433, 297-304. <https://doi.org/10.1002/zaac.19774330137>
64. L. Z. Liu, M. Yu, X. Y. Li, Q. P. Kang, and W. K. Dong. *Chin. J. Inorg. Chem.*, **2019**, 35, 1283-1294.
65. X. Xu, R. N. Bian, S. Z. Guo, W. K. Dong, and Y. J. Ding. *Inorg. Chim. Acta*, **2020**, 513, 119945. <https://doi.org/10.1016/j.ica.2020.119945>
66. J. F. Wang, R. Y. Li, P. Li, and W. K. Dong. *Inorg. Chim. Acta*, **2021**, 518, 120247. <https://doi.org/10.1016/j.ica.2021.120247>
67. M. A. Spackman and D. Jayatilaka. *CrystEngComm*, **2009**, 11, 19-32. <https://doi.org/10.1039/B818330A>
68. P. Manna, S. K. Seth, A. Das, J. Hemming, R. Prendergast, M. Helliwell, S. R. Choudhury, A. Frontera, and S. Mukhopadhyay. *Inorg. Chem.*, **2012**, 51, 3557-3571. <https://doi.org/10.1021/ic202317f>